Postprint of: Niedziałkowski P., Jurczak P., Orlikowska M., Wcisło A., Ryl J., Ossowski T., Czaplewska P., Phospholipid-functionalized gold electrode for cellular membrane interface studies - interactions between DMPC bilayer and human cystatin C, Biochimica et Biophysica Acta (BBA) - Biomembranes, Vol. 1866, Iss. 3 (2024), 184266, DOI: 10.1016/j.bbamem.2023.184266

Phospholipid-functionalized gold electrode for cellular membrane interface studies - interactions between DMPC bilayer and human cystatin C

Paweł Niedziałkowski[a]*, Przemysław Jurczak[b, c]**, Marta Orlikowska[b], Anna Wcisło[a], Jacek Ryl[d], Tadeusz Ossowski[a], Paulina Czaplewska[c]

[a] Department of Analytical Chemistry Faculty of Chemistry, University of Gdansk, Wita Stwosza 63, Gdańsk, 80-308, Poland

[b] Department of Biomedical Chemistry, Faculty of Chemistry, University of Gdansk, Wita Stwosza 63, Gdańsk, 80-308, Poland

[c] Specialist Laboratories, Intercollegiate Faculty of Biotechnology UG&MUG, Abrahama 58, Gdańsk, 80-307, Poland

[d] Division of Electrochemistry and Surface Physical Chemistry, Institute of Nanotechnology and Materials Engineering and Advanced Materials Center, Gdańsk University of Technology, Narutowicza 11/12, Gdańsk, 80-233, Poland

* Correspondence to: P. Niedziałkowski, Department of Analytical Chemistry Faculty of Chemistry, University of Gdansk, Wita Stwosza 63, Gdańsk, 80-308, Poland

** Correspondence to: P. Jurczak, Department of Biomedical Chemistry, Faculty of Chemistry, University of Gdansk, Wita Stwosza 63, Gdańsk, 80-308, Poland, Specialist Laboratories, Intercollegiate Faculty of Biotechnology UG&MUG, Abrahama 58, Gdańsk, 80-307, Poland

E-mail addresses pawel.niedzialkowski@ug.edu.pl, (P. Niedziałkowski), przemyslaw.jurczak@ug.edu.pl (P. Jurczak)

Abstract: This work describes the electrochemical studies on the interactions between V57G mutant of human cystatin C (hCC V57G) and membrane bilayer immobilized on the surface of a gold electrode. The electrode was modified with 6-mercaptohexan-1-ol (MCH) and 1,2-dimyristoyl-sn-glycero-3-phosphocholine (DMPC). DMPC was used as a membrane mimetic for monitoring electrochemical changes resulting from the interactions between the functionalized electrode surface and human cystatin C. The interactions between the modified electrode and hCC V57G were investigated by cyclic voltammetry and electrochemical impedance spectroscopy in a phosphate buffered saline (PBS) containing $Fe(CN)_6^{3-/4-}$ as a redox probe. The electrochemical measurements confirm that fabricated electrode is sensitive to hCC V57G at the concentration of 1×10^{-14} M. The incubation studies carried out at higher concentrations resulted in insignificant changes observed in cyclic voltammetry and electrochemical impedance spectroscopy measurements. The calculated values of surface coverage θ_R confirm that the electrode is equally covered at higher concentrations of hCC V57G. Measurements of wettability and surface free energy made it possible to determine the influence of individual structural elements of the modified gold electrode on its properties, and thus allowed to understand the nature of the interactions. Contact angle values confirmed the results obtained during electrochemical measurements, indicating the sensitivity of the electrode towards hCC V57G at the concentration of 1×10^{-14} M. In addition, the XPS spectra confirmed the successful anchoring of hCC V57G to the DMPC-functionalized surface.

Keywords: human cystatin C, DMPC, phospholipid, membrane, 6-Mercaptohexan-1-ol, electrode modification

1. Introduction

An amyloid is an insoluble, aggregated form of a protein or peptide, which assumes a fiber-like shape [1]. The process of accumulation and deposition of amyloid is a hallmark of amyloid diseases, a group of pathological states exhibiting various symptoms, e.g., Parkinson's or Alzheimer's disease. Up to date about forty amyloid-forming peptides and proteins were described [2]. Among them we find human cystatin C (hCC), a small size (120 amino acid-long) inhibitor of cysteine proteinases [3]. This protein with physiologic isoelectric point of pH 9.3 [4] can be found in all human body fluids at physiologically relevant concentrations [5]. Despite the physiological relevance of the wild-type hCC as a regulator of the activity of inter- and intramolecular cysteine proteases, its Leu^{68}→Gln mutant is prone for accumulation, causing a dominant hereditary disorder called hereditary cystatin C amyloid angiopathy, a disease characterized by brain strokes and death of patients at a young age [6].

Even though the processes leading to amyloidogenic diseases are not crystal clear, it is known that protein oligomerization is a key feature of the amyloid formation. Research indicates that biological membranes have a great impact on the process of amyloidogenic proteins' oligomerization [7–9]. Up to date two possible mechanisms of protein oligomerization were proposed [10]. The first one assumes that the protein oligomerizes in extracellular matrix. The second, that the membrane is the interface which facilitates and accelerates the whole process. Both ideas involve different oligomeric states of a protein and finally lead to the formation of fibrils [10]. An annular oligomer is one of the oligomeric states on the route to the fibril formation. It may form channels in biological membranes disturbing their integrity, therefore it is indicated as a potential cause of toxicity of amyloidogenic proteins [10]. The formation of annular oligomers was observed for different amyloidogenic proteins i.e. amyloid β peptide [11], immunoglobulin light chain [12] and human cystatin C [13]. The interaction of toxic forms of hCC (the protein of our interest) with biological membranes is an interesting aspect of studies on amyloidogenic diseases and may be crucial in the context of describing the mechanisms causing them.

The studies on interactions between proteins and membranes are not a trivial task. Biological membranes are complex multi-component structures, therefore to facilitate experimental measurements natural membranes are often substituted with model structures including micelles, bicelles and liposomes [14,15]. Different methods involving the use of natural and model membranes have been developed. Among others we find surface plasmon resonance (SPR) [16], isothermal titration calorimetry (ITC) [17], nuclear magnetic resonance (NMR) spectroscopy[15], Fourier transform infrared spectroscopy (FTIR) [18], hydrogen-deuterium exchange (HDX) mass spectrometry [19] or molecular dynamics (MD) simulations [20]. These techniques include also such interesting concepts as monitoring of resonance frequency and energy dissipation on lipid covered quartz crystal (microbalance) resulting from a contact/interaction with a protein [21] or the use of anisotropy of nuclear interactions (solid-state NMR) to determine protein structure within solid or semi-solid lipid membrane structures [22]. Some of the methods applied for protein-membrane interactions present such a broad range of application or particular design, that they can be applied for studies on soluble proteins as well as protein aggregates and fibrils (i.e., amyloid fibrils), which often prove to be tricky study objects due to their low solubility. These techniques comprise i.a. total internal reflection ellipsometry (TIRE) [23], Förster resonance energy transfer (FRET) [24], fluorescence imaging [25], quartz crystal microbalance applications [26] or MD simulations [27]. The technique which seems to be exploited the most in the field of protein-membrane interactions, regardless of the oligomeric state of the studied molecule, is atomic force microscopy (AFM). It allowed, e.g., to visualize aggregation of α-synuclein on a surface of phospholipid bilayers and (combined with computational modeling) to present a possible model of aggregation of this amyloidogenic protein [28]. AFM imaging was also applied to visualize the formation of annular oligomers (amyloid fibril precursors) forming transmembrane channels [29].

All the mentioned techniques shine bright in some aspects of application and falter in others. One of the greatest disadvantages of many mentioned above (e.g., NMR, ITC, SPR) is their high cost, resulting from relatively high amount of protein/membrane material required for the measurement and/or high cost of the measurement itself. Therefore, here the application of electrochemical impedance spectroscopy (EIS) and cyclic voltammetry (CV) as methods for studies on protein-membrane interactions based on V57G mutant of hCC and the DMPC membrane mimetic is presented.

The hCC protein was previously detected with electrochemical methods including cyclic voltammetry (CV) and differential pulse voltammetry (DPV) on screen printed electrode modified with papain (cysteine protease) [30] or carbon electrode functionalized with graphene oxide-chitosan (GO-Chit) and with anti–cystatin C antibody [31]. The hCC was also detected with CV and DPV methods on glassy carbon electrode covered with aminoferrocene (Fc), graphene oxide (GO) polyethyleneimine (PEI) film and anti-cystatin C antibody, without the use of redox probes during electrochemical measurements [32]. The above mentioned methods were also used to detect hCC on synthetic plastic antibody for hCC designed with the molecularly imprinted polymer (MIP) technique on a carbon screen-printed electrode [33]. The EIS method was previously used for hCC detection only using the electrochemical immunosensor based on interdigitated electrode (IDE) modified with polypyrrole/carbon nanotube nanoyhibrid film and monoclonal antibodies anti-CysC [34].

However, to our knowledge, the EIS technique has not yet been suggested before for studies on interactions between hCC and membrane surface or protein-membrane interactions, exploiting a gold electrode. Nevertheless there are reports concerning the modification of gold electrodes for the purpose of detecting proteins in bacterial membrane extracts with the EIS and CV techniques [35]. Additionally, the interactions between amyloid β monomers (AβMs) and amyloid β oligomers (AβOs) and a floating bilayer lipid membrane (fBLM) using gold electrodes were previously studied with EIS and IR spectroscopy techniques [36].

In this study a gold electrode modified with the 6-Mercaptohexan-1-ol (MCH) and DMPC membrane mimetic was applied for monitoring electrochemical changes resulting from the interaction between the functionalized electrode surface and V57G variant of hCC at concentrations ranging from 1×10^{-14} M to 1×10^{-6}. The electrochemical changes were monitored with EIS and CV techniques. The CV results indicate that the most significant current changes were evident after incubation in a solution containing hCC V57G at the concentration of 1×10^{-14}. The EIS measurements confirmed the CV data. The most significant changes in charge transfer resistance were observed for the hCC V57G solution at the concentration of 1×10^{-14} M. The incubation of electrode in hCC V57G solutions at higher concentration caused insignificant changes observed in electrochemical impedance spectra. Additionally, the calculated surface coverage θ_R confirmed that the electrode is coated in a similar manner for incubation studies in solutions at concentrations ranging from 1×10^{-12} M to 1×10^{-6} M. The modification of electrode surface and interactions between DMPC and hCC V57G were studied with the high-resolution X-ray photoelectron spectroscopy (XPS) and contact angle and surface free energy measurements.

2. Methods and materials

2.1. Materials and reagents

All solvents and reagents were used as received without further purification. 6-mercaptohexan-1-ol (MCH), 1,2-dimyristoyl-*sn*-glycero-3-phosphocholine (DMPC), $K_3[Fe(CN)_6]$ and $K_4[Fe(CN)_6]$ were purchased from Sigma-Aldrich.

2.2. Expression and purification of human cystatin C

The DNA of hCC V57G variant was obtained with site-directed mutagenesis as previously described [3]. Plasmid DNA (pHD313 vector [37]) including hCC gene coupled with signal peptide delivered from *E. coli* OmpA protein (responsible for secretion of hCC into the periplasmatic space), temperature-sensitive λ cI 857 repressor, λ PR promoter and ampicillin resistance gene was expressed in *E. coli* BL21(DE3) competent cells according to earlier described-protocol [3].

2.3. DMPC phospholipid bilayer preparation

The lyophilized DMPC powder was suspended in PBS buffer (Sigma Aldrich). The phospholipid suspension was subjected to 15 incubation cycles involving 30 min incubation in ultrasound bath with heating (313 K) and 30 min incubation in 277 K. This procedure allowed to obtain stable, homogenous, and transparent solution of double-layered lipid bilayers. For the purpose of the experiment, 10 mM DMPC liposome stock solution was prepared and used for the preparation of a dilution series.

2.4. Functionalization of gold electrodes

The gold electrodes of 1.6 mm diameter used for all measurements were purchased from (Mineral, Poland). Before each modification, the electrodes were carefully polished using polishing pad saturated with micro polish alumina powder (1.0 μm; Buehler, USA). Then the electrodes were washed, dried in a stream of air, and placed in the vessel containing 1 mL of 1 mM MCH dissolved in absolute ethanol in order to obtain self-assembly monolayer on electrode surface. After 16 h the electrodes were washed with ethanol and dried. Afterwards, the electrode was modified with a layer of DMPC via incubation of its surface in 10 μL of 1 μM solution of DMPC for 1 h. The DMPC concentration used for electrode modification was higher than the critical micelle concentration (CMC) value (6nM), to ascertain the formation bilayer of DMPC on the electrode. The electrodes obtained in above manner were incubated in the hCC V57G solution at ascending concentrations ranging from 1×10^{-14} M to 1×10^{-6} M for 50 minutes. After each electrochemical measurement the electrodes were rinsed with a 0.01 M PBS solution, pH 7.4.

The gold electrodes of 11 mm x11 mm used in an XPS, contact angle and surface free energy experiments were purchased from (Arrandee, Germany). Before use the electrodes were incubated in a concentrated sulfuric acid for 4 minutes, washed with water and ethanol and modified according to the same procedure as described above for gold electrodes of 1.6 mm diameter.

2.5. X-ray photoelectron spectroscopy measurements

X-ray photoelectron spectroscopy (XPS) analyses were carried out using the Escalab 250Xi spectroscope (ThermoFisher Scientific) utilizing AlKα X-ray spot, diameter 500 μm. The pass energy was set up to 20 eV. The low-energy electron and low-energy Ar^+ ion bombardment were used for charge compensation with final peak calibration using adventitious C1s (284.6 eV). Peak deconvolution was performed in Avantage v.59921 provided by spectroscope manufacturer.

2.6. Contact angle and surface free energy measurements

The Drop Shape Analyzer – DSA100 by Krüss was used to determine the contact angle and surface free energy of investigated samples. The contact angles of drops of four different liquids (water, formamide, glycerol, and diiodomethane) were measured to determine the surface free energy. The image of a 4 μL drop of the probe liquid deposited using a syringe was captured by a camera and after the digital image analysis, the average contact angle was deduced using the Young-Laplace method from the angles measured at both sides of the drop in equilibrium. The measurements were repeated 20 times. The total surface free energy γs and its dispersive γd and polar γp components of the surfaces were determined by the Owens, Wendt, Rabel, and Kaelble (OWRK) method from the contact angles of the three liquid drops (water, formamide and diiodomethane) [38–40].

2.7. Electrochemical impedance spectroscopy and cyclic voltammetry measurements

The cyclic voltammetry (CV), and electrochemical impedance spectroscopy (EIS) measurements were performed using M204 multichannel potentiostat (Autolab, Netherlands) equipped with FRA32M electrochemical impedance spectroscopy module in a three-electrode cell. The unmodified and modified gold electrodes served as working electrodes, Ag/AgCl (0.1 M KCl) was a reference electrode and platinum wire was a counter electrode. All electrochemical measurements were performed in 0.01 M PBS solution of pH 7.0 containing $Fe(CN)_6^{3-/4-}$ as redox probes, containing 1 mM $K_3[Fe(CN)_6]$ and 1 mM $K_4[Fe(CN)_6]$ (1 : 1). The cyclic voltammograms were obtained at scan rate of 0.1 V/s. The EIS spectra were obtained with frequency range of 0.1 Hz to 10 kHz, at with perturbation amplitude of 10 mV, at the open circuit potential (OCP). All the spectra were analyzed using ZSimpWin 3.21 impedance analysis software. All EIS spectra were fitted using modified Randles equivalent circuit $R_s(Q(R_{ct}W))$, where R_s is electrolyte resistance, Q_{dl} – constant phase element, R_{ct} – charge transfer resistance, and W – Warburg element.

3. Results and discussion

3.1. The gold electrode modification procedure

The gold electrodes used for detection of hCC V57G were modified according to the scheme shown in Figure 1a. The crystallographic structure of hCC V57G presented in Figure 1 was previously reported in [41]. In the first stage of the modification process MCH was applied to create a stable self-assembled monolayers (SAMs) on the gold electrode surface due to the fact that, it forms an organized layer on the electrode [42]. The SAMs formation is usually used in the first step of the process of electrode functionalization for construction of electrochemical sensors and biosensors [43–45]. In this work 1 mM ethanolic solution of MCH was used for electrode modification. The modification of gold electrodes with MCH takes place not only in ethanolic solution [46], but also in an aqueous solutions [47] or buffer solutions [48]. During the second stage the gold electrode was modified with DMPC by immersing electrode in 1 μM DMPC solution in PBS for 1 h. The chemical structure of the DMPC membrane is shown in Figure 1b. The electrode fabricated in this procedure was directly applied to measurements using CV and EIS methods.

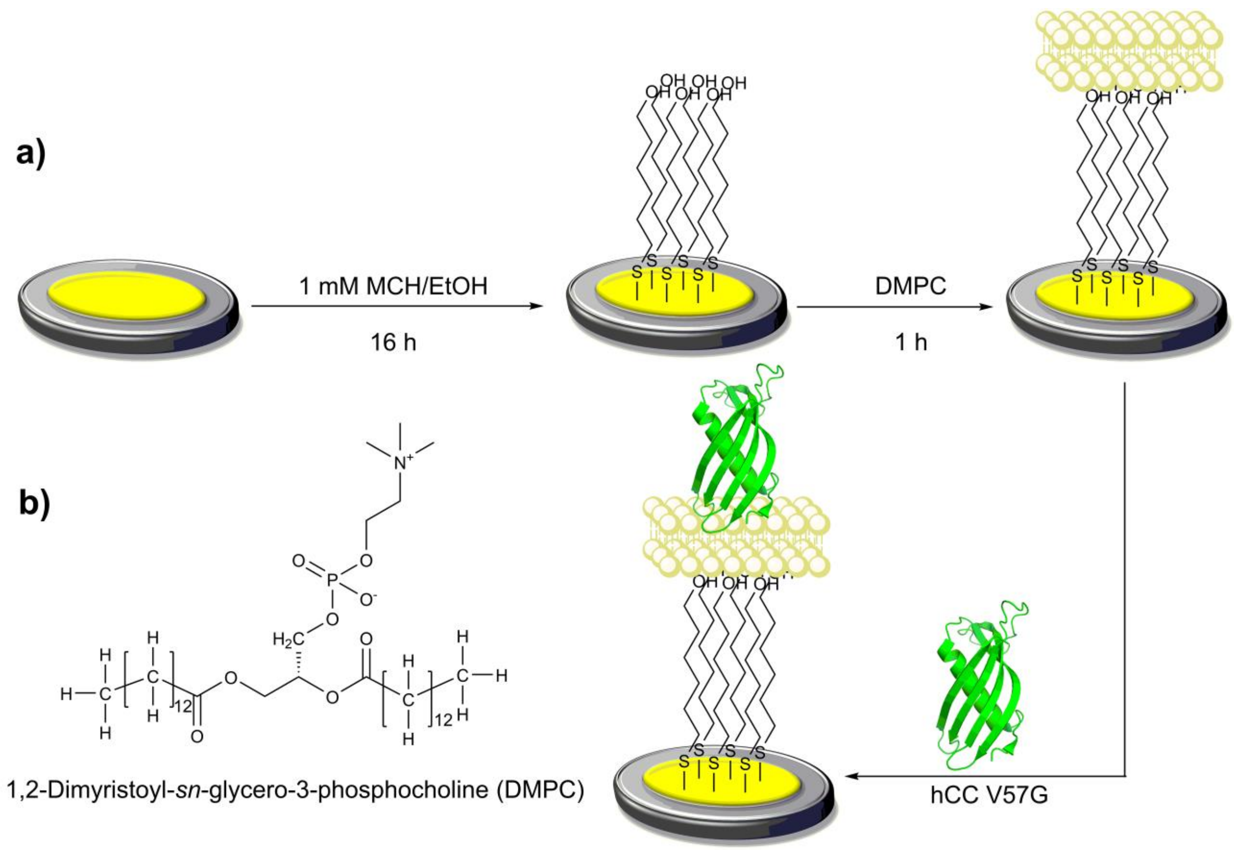

Figure 1. (a) The modification of gold electrode with MCH and DMPC for the hCC V57G detection. (b) The chemical structure of DMPC.

3.2. XPS Measurements

The XPS spectra were registered to analyze Au electrode surface chemistry and confirm the successful anchoring of hCC V57G to the DMPC-functionalized surface. The results of XPS analysis for primary film constituents are presented in Figure 2.

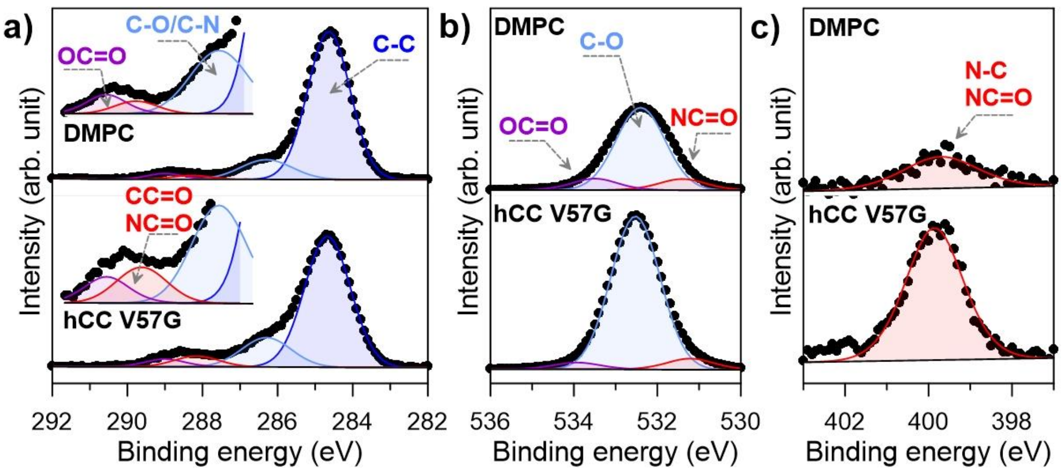

Figure 2. High-resolution XPS measurements of the electrode surface after DMPC and hCC functionalization steps, studied in the core-level binding energy range of (a) C1s, six times enhanced in the inset, (b) O1s, and (c) N1s with proposed deconvolution model.

The dominant component of the C1s spectra (Figure 2a) is C-C aliphatic bond (284.6 eV) within the DMPC and hCC V57G. Furthermore, three additional components can be distinguished, representing different oxidized forms of organic carbon. Their peak positions are characteristic for C-O and C-N interactions (286.3 eV), aliphatic esters, carbonyls, amides, imides (288.3 eV), and carboxyl groups (289.0 eV). The share of all oxidized species in total [C] equals 18.0 % in case of DMPC and increases significantly, reaching even 27.3 % after hCC V57G anchoring. Here, the share of the C=O/NC=O moieties increases the most, from 2.8 up to 5.9 % of total [C]. Unfortunately, the signals representing single phosphorus atoms from within DMPC structure or S atom present in the thiol groups were too low for the threshold of the spectroscope and were not detected. The detailed deconvolution analysis is presented in

Table 1.

Table 1. Results of XPS data deconvolution (in at.%).

	C1s				O1s			N1s
	C-C	C-O	C=O/ NC=O	OC=O	NC=O	C-O	OC=O	N-C/ NC=O
BE (eV)	284.6	286.3	288.2	289.0	531.2	532.5	533.9	399.9
DMPC	46.1	7.5	1.6	1.1	33.9	4.6	4.5	0.7
hCC V57G	24.7	5.9	1.3	2.0	57.5	4.2	2.5	1.9

The above-mentioned observations are assisted by a tremendous rise in oxygen content, analyzed based on the O1s spectra (Figure 2b). The total share of all [O] species increases from 43.0 up to 64.21 at.%, when $C_{580}H_{910}N_{170}O_{176}S_7$ (hCC V57G) is anchored to the modified electrode surface. The surface modification with hCC V57G particularly affects the C-O bonds (O1s at 532.5 eV), which corroborate with the findings observed from the C1s peak analysis. Moreover, over two-fold increase in the N1s share, from 0.7 to 1.9 at.% was also observed. The N1s peak used for the deconvolution is located at 399.9 eV, a value characteristic for amide or imides but also amines.

3.3. Contact angle and surface free energy measurements

Wettability measurements at the modified gold electrode surface allowed to determine the influence of the modification process on the characteristics of the tested systems (Figure 3). The obtained results clearly indicate that the modification of the gold electrode with MCH causes a significant change in its properties. The decrease in the contact angle from 78.5° for the bare electrode to 30.6° for the 1-hexanethiol-modified surface is a significant change. The presence of MCH made the surface more hydrophilic, which is the result of the presence of -OH groups on the modified electrode surface. The introduction of the DMPC membrane into the system, in turn, causes an increase in hydrophobicity, which is manifested in an increase in the contact angle to 41.3° (Figure 3a). Further studies showed that the interaction with hCC V57G is visible for the concentration of 10^{-14} M. For electrodes incubated in such protein concentration, we observe a decrease in hydrophobicity by approx. 7° compared to electrodes with a DMPC membrane. In turn, the electrodes incubated in higher hCC V57G concentrations showed only slight changes in the contact angle (approx. 1-2°). This clearly indicates that the electrode is sensitive only below the concentration of 1×10^{-14} M.

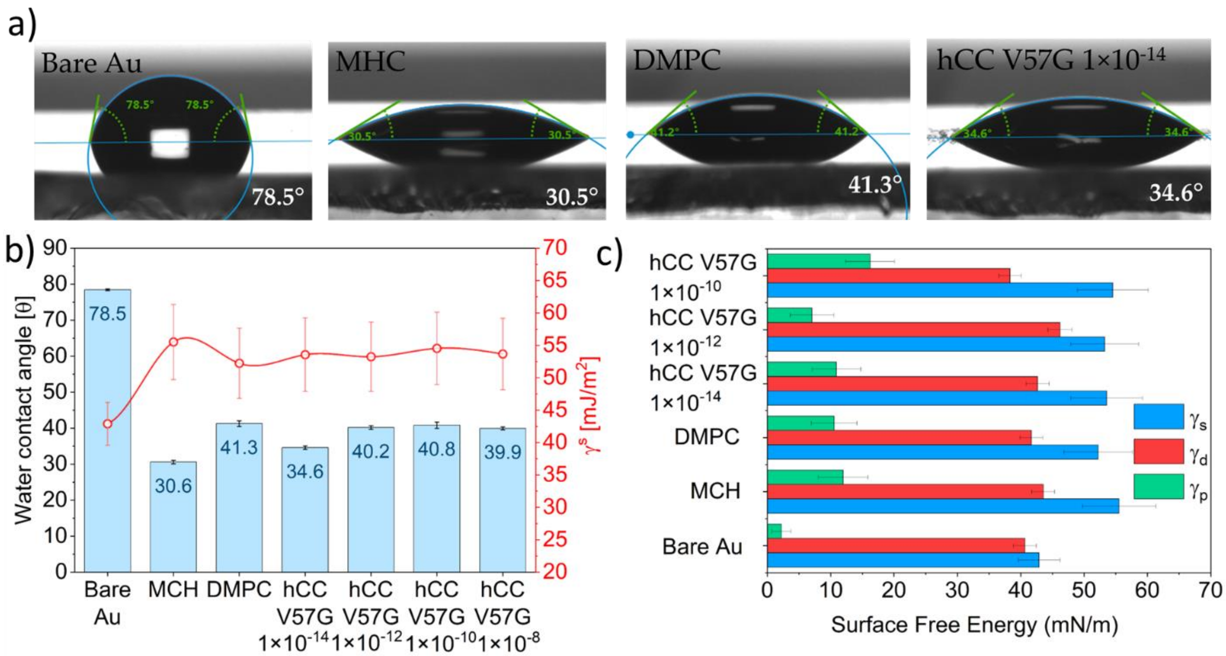

Figure 3. (a) Wettability measurement photos, (b) water contact angle (blue bar) and surface free energy γs (red line), and (c) surface free energy γs diagram (blue bar) with disperse (red bar) and polar (green bar) parts, for each step of the modification of the gold electrode for hCC V57G sensing.

Surface free energy allows to determine the biocompatibility of a given system, as well as to track the interactions or physicochemical changes resulting from the interactions of the system with the analyte. The modification of the gold electrode with a thiol layer increases the surface free energy (around 15 mN/m) (Figure 3b,c). This is due to a significant increase in the share of the polar part (Figure 3c), resulting from the appearance of functional groups on the surface of the electrode, which were not present in the case of a bare electrode. Further anchoring of the DMPC membrane on the thiol surface reduces the free energy, but only by about 5 mN/m (Figure 3c). Such an effect may be caused by the arrangement of the lipid bilayer formed by DMPC. Changes in the contact angle and surface free energy (Figure 3b) indicate that the membrane surface has hydrophilic heads pointing outward from the layer. Hence, the hydrophilic character of the system is maintained, although it is weaker compared to the thiol layer rich in -OH groups. In the case of surface free energy parameters, we do not observe such a large variability in the presence of interaction with hCC V57G as in the case of the contact angle value. Nevertheless, the share of both dispersive and polar interactions (hydrogen bonding and dipole-dipole interactions) is visible.

3.4. Electrochemical measurements

3.4.1. Cyclic voltammetry (CV)

The cyclic voltammetry (CV) was used to characterize the response of an electrode during the modification steps and in order to examine the electrode after incubation in hCC V57G solutions at concentrations ranging from 1×10^{-14} M to 1×10^{-6} M. Figure 4a shows the cyclic voltammograms obtained for bare gold electrode before and after modification with MCH and DMPC. All measurements were performed in 0.01 M PBS solution (pH 7.0) containing 1 mM $Fe(CN)_6^{3-/4-}$ used as redox probe. The two reversible peaks are observed on cyclic voltammograms with peak-to-peak separation (ΔE) of 76 mV. The intensity current of peaks decrease after modification with MCH with the peak-to-peak separation increasing to 159 mV, suggesting the SAMs formation on the electrode surface. Similar value of (ΔE) was observed in the previous paper indicating the formation of monolayer on a gold electrode [49]. Further functionalization of the electrode with DMPC leads to an even greater decrease in current intensity and an increase in peak-to-peak separation to 214 mV. The above-mentioned changes indicate that electron transfer to the surface of the electrode has been inhibited, indicating that its surface has been modified. The cyclic voltammograms of the modified electrode after incubation in PBS solution containing different concentrations of hCC V57G are shown in Figure 4b. The incubation in 1×10^{-14} M hCC V57G solution causes a slight decrease in anodic peak and a shift in the position of the cathodic peak, with peak-to-peak separation (ΔE) of 250 mV relative to the voltammogram observed for DMPC. The changes observed in the cyclic voltammograms for hCC V57G at the concentration of 1×10^{-14} M are most significant. Further incubation in a solution containing 1×10^{-12} M hCC V57G solution causes further decrease in the current intensity and an increase of (ΔE) to 311 mV. At the same time, after incubation in hCC V57G solutions at the concentration of 1×10^{-10} M and 1×10^{-8} M, almost identical voltammograms were obtained with ΔE of 362 mV and 359 mV respectively. The incubation in 1×10^{-6} M hCC V57G solution also does not cause changes in the peak heights, only a shift of the anode peak towards negative values is observable resulting in ΔE decrease to 329 mV. The CV analysis indicates that the most significant changes are observed after incubation of the electrode in 1×10^{-14} M hCC V57G solution.

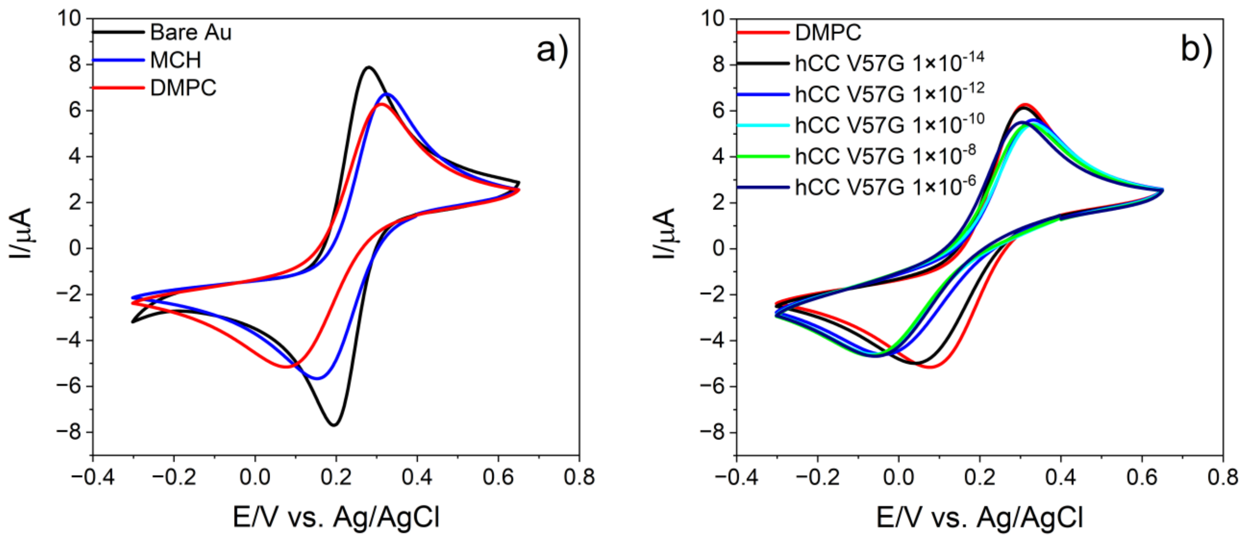

Figure 4. (a) Cyclic voltammograms of bare Au electrode and electrodes modified with MCH and DMPC. (b) Cyclic voltammograms of the DMPC-modified electrode after incubation in hCC V57G solutions at concentrations ranging from 1×10^{-14} M to 1×10^{-6} M recorded in 0.01 M PBS (pH 7.0) containing 1 mM $Fe(CN)_6^{3-/4-}$,scan rate 100 mV/s.

3.4.2. Electrochemical Impedance Spectroscopy (EIS)

The EIS measurements were performed in 0.01 M PBS solution (pH 7.0) containing $Fe(CN)_6^{3-/4-}$. Figure 5a shows the impedance spectra obtained for bare Au electrode, electrode modified with MCH, electrode modified with DMPC and the modified electrodes after incubation in hCC V57G solutions at concentrations ranging from 1×10^{-14} M to 1×10^{-6} M. All spectra were fitted using modified Randles equivalent circuit $R_s(Q_{dl}(R_{ct}W))$. The charge transfer resistance calculated for a bare electrode (R_{ct} = 1.003 kΩ) increases significantly after modification with MCH to (R_{ct} = 12.970 kΩ) with the decreases of constant phase element (Q_{dl}) from 1.426 µF for bare Au electrode to 0.191 µF after MCH modification. A similar phenomenon was also observed in previous work [49]. The Au electrode coated with MCH additionally modified with DMPC causes an increase of R_{ct} to 18.530 kΩ and increase of constant phase element (Q_{dl}) to 0.212 µF (see Table S1 in Supplementary Information). Further incubation in hCC V57G solutions at the concentrations of 1×10^{-14} M cause an increase of the charge transfer resistance R_{ct} to 25.180 kΩ. A subsequent incubation in hCC V57G solutions at higher concentrations causes an increase of R_{ct} to 37.400 kΩ after incubation in 1×10^{-12} M hCC V57G and remains constant (37.520 kΩ) for 1×10^{-6} M hCC V57G solution. It's also worth noting that after DMPC modification the parameter n is constant regardless of any incubation in hCC V57G solution and is close to 1 [36]. This indicates that the surface roughness does not change significantly during subsequent stages of hCC V57G detection at different concentrations [50]. The understanding of the mechanism of interactions between the DMPC layer immobilized on the gold electrode and hCC V57G at different concentrations requires additional research. Nevertheless, the previous EIS studies on interaction between amyloid β monomers (AβMs) and the floating bilayer lipid membrane (fBLM) do not lead to the formation of pores. Only the β oligomers (AβOs) induced the pore formation in examined membrane [36].

Figure 5b shows the ΔR_{ct} correlation, where ΔR_{ct} was calculated as difference between the R_{ct} after electrode incubation in hCC V57G solutions of different concentration and R_{ct} of DMPC and the logarithm of the hCC V57G concentration. The above relationship clearly shows that the calculated change in ΔR_{ct} for the electrode after incubation in 1×10^{-14} M hCC V57G solution reaches a value of 6.650 kΩ, then rapidly increases to 18.870 kΩ after incubation in 1×10^{-12} M hCC V57G solution . Subsequent incubations in higher concentrations of hCC V57G result in only slight changes in ΔR_{ct} values, suggesting that the resulting electrode is not so sensitive to the presence of hCC V57G at the higher concentrations ranging from 1×10^{-12} M to 1×10^{-6} M.

Figure 5c shows the plot of surface coverage θ_R after each step of bare Au modification, calculated according to the following equation $\theta_R = 1 - (R_{ct\ (Bare\ Au)} / R_{ct\ (Modified\ Au)})$ [51,52], where $R_{ct\ (Bare\ Au)}$ and $R_{ct\ (Modified\ Au)}$ corresponds to the charge transfer resistance for the bare electrode and the appropriately modified electrodes respectively. The surface coverage of gold electrode after SAMs formation was 0.923, while after DMPC modification the surface coverage increased to 0.946, then after incubation in hCC V57G solution at the concentration of 1×10^{-14} M the surface coverage was 0.960. The incubations of the modified gold electrode in hCC V57G solution with concentrations ranging from 1×10^{-12} M to 1×10^{-6} M did not change the electrode coverage. The calculated surface coverage value for each electrode was constant at 0.973. The 0.97 degree coverage of the electrode surface may indicate that pores can be present on the bilayer of DMPC deposited on the electrode, which allows the redox probe to reach the electrode. This unequivocally proves that the gold electrode used in this study shows the most significant changes after incubation in the solution of hCC V57G at concentration of 1×10^{-14} M. The lack of significant changes above the concentrations of 10^{-14} M of hCC V57G can be attributed to the saturation of binding sites on the electrode surface. The previously published data shows that only an external random coil loop region of hCC protein interacts with DMPC bilayer and the protein does not migrate into the bilayer, but interacts with its surface [15].

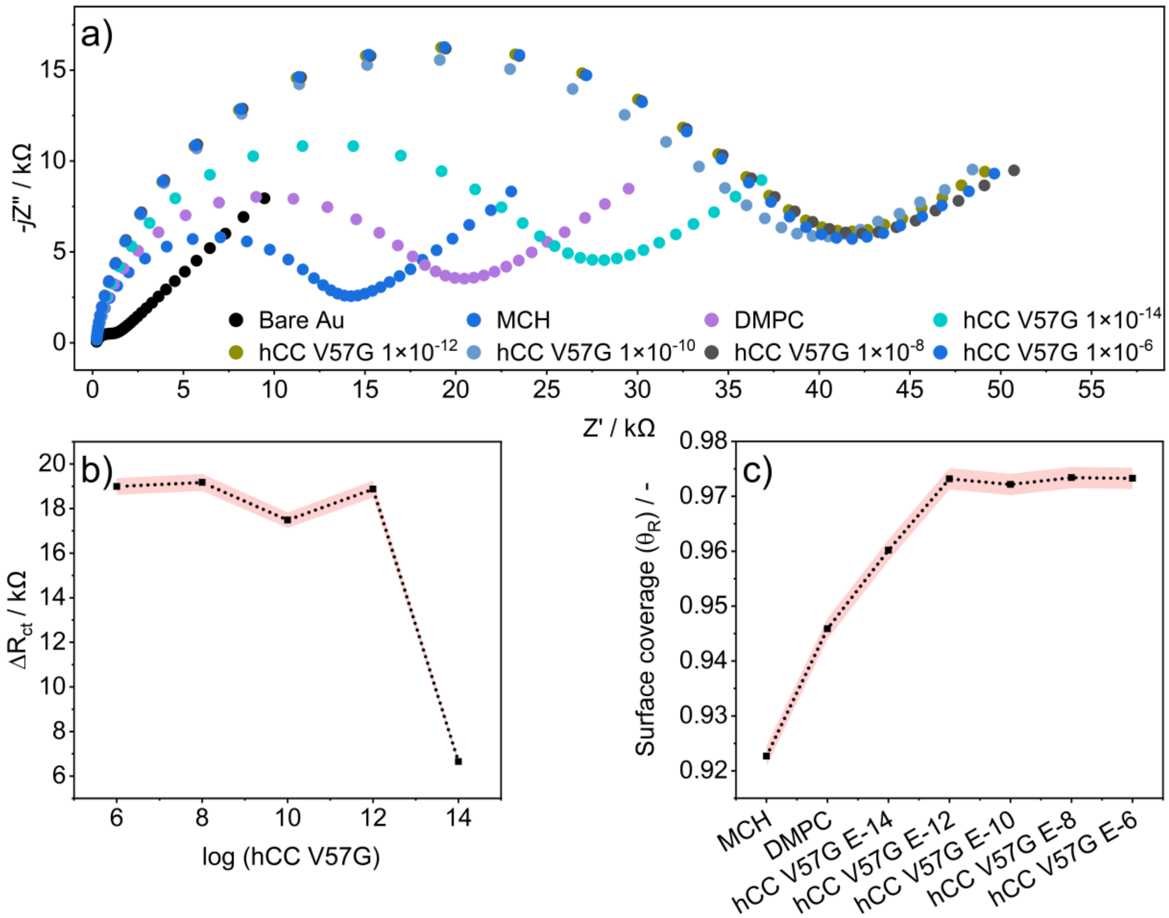

Figure 5. The electrochemical impedance spectra obtained for (a) bare Au electrode, electrodes modified with MCH and DMPC and modified electrodes after incubation in hCC V57G solutions at concentrations ranging from 1×10^{-14} M to 1×10^{-6} M. (b) Correlation between ΔR_{ct} and the logarithm of the hCC V57G concentration. (c) The electrode surface coverage after each step of modification. The red lines indicate the error bars.

CV and EIS technique have not been applied before for studies on interactions between hCC and membrane surface or protein-membrane interactions with the use of gold electrodes. The presented studies proves that the CV and EIS methods can be applied for the monitoring of changes occurring on the surface of an electrode modified with the DMPC bilayer during incubation in the V57G solution at different concentrations. EIS measurements also indicate that the hCC V57G can be detected at the concentrations ranging from 1×10^{-14} M to 1×10^{-6} M, nevertheless the most significant changes were observed for the hCC V57G at the concentration of 1×10^{-14} M.

4. Conclusion

The presented research indicates that the gold electrode modified with MCH and DMPC bilayer, allows for monitoring the interactions between DMPC and V57G mutant of human cystatin C. The interactions between the modified electrode and the hCC V57G protein were monitored at concentrations ranging from 1×10^{-14} M to 1×10^{-6} M. Both the CV and EIS measurements indicate that the most significant changes were observed for the protein detection at the concentration of 1×10^{-14} M. The incubation in hCC V57G solutions at higher concentration did not cause any changes relevant in the experimental conditions. Furthermore, the EIS measurements indicate that incubation of the modified electrode in hCC V57G solutions, at concentrations ranging from 1×10^{-12} M to 1×10^{-6} M, did not change the electrode coverage. The electrochemical data obtained in this study were also confirmed with water contact angle and surface free energy measurements. The decrease in contact angle upon MCH modification highlights the enhancement of surface hydrophilicity, while the subsequent increase in contact angle after the addition of the DMPC membrane signifies the increase of hydrophobicity of the modified surface. The sensitivity of the electrode in relation to the interaction with hCC V57G at different concentrations was reflected in the contact angle measurements. The most noticeable decrease in hydrophobicity (by approximately 7°) was observed for electrodes incubated with hCC V57G at the concentration of 10^{-14} M. Obtained results confirm that the presented method of electrode functionalization allows to monitor the interactions between the electrode surface and hCC V57G protein.

Declaration of interests

The authors declare that they have no known competing financial interests or personal relationships that could have appeared to influence the work reported in this paper.

Acknowledgements

This work was financially supported by Harmonia 10 grant (2018/30/M/ST4/00039) from National Science Centre, Poland. We thank Prof. Artur Zieliński and Prof. Robert Szoszkiewicz for scientific discussions and Weronika Janik for technical support.

6. Reference

[1] M.D. Benson, J.N. Buxbaum, D.S. Eisenberg, G. Merlini, M.J.M. Saraiva, Y. Sekijima, J.D. Sipe, P. Westermark, Amyloid nomenclature 2018: recommendations by the International Society of Amyloidosis (ISA) nomenclature committee, Amyloid, 25 (2018) 215–219.

[2] M.D. Benson, J.N. Buxbaum, D.S. Eisenberg, G. Merlini, M.J.M. Saraiva, Y. Sekijima, J.D. Sipe, P. Westermark, Amyloid nomenclature 2020: update and recommendations by the International Society of Amyloidosis (ISA) nomenclature committee, Amyloid, 27 (2020) 217–222.

[3] A. Szymańska, A. Radulska, P. Czaplewska, A. Grubb, Z. Grzonka, S. Rodziewicz-Motowidło, Governing the monomer-dimer ratio of human cystatin c by single amino acid substitution in the hinge region, Acta Biochim. Pol., 56 (2009).

[4] A. Onopiuk, A. Tokarzewicz, E. Gorodkiewicz, Cystatin C: a kidney function biomarker, Adv. Clin. Chem., 68 (2015) 57–69.

[5] M. Abrahamson, A.J. Barrett, G. Salvesen, A. Grubb, Isolation of six cysteine proteinase inhibitors from human urine Their physicochemical and enzyme kinetic properties and concentrations in biological fluids, J. Biol. Chem., 261 (1986) 11282–11289.

[6] I. Ekiel, M. Abrahamson, Folding-related Dimerization of Human Cystatin C (∗), J. Biol. Chem., 271 (1996) 1314–1321.

[7] M.F.M. Sciacca, C. Tempra, F. Scollo, D. Milardi, C. La Rosa, Amyloid growth and membrane damage: Current themes and emerging perspectives from theory and experiments on Aβ and hIAPP, Biochim. Biophys. Acta BBA - Biomembr., 1860 (2018) 1625–1638.

[8] A. Vahdat shariat panahi, P. Hultman, K. Öllinger, G.T. Westermark, K. Lundmark, Lipid membranes accelerate amyloid formation in the mouse model of AA amyloidosis, Amyloid, 26 (2019) 34–44.

[9] M.S. Terakawa, Y. Lin, M. Kinoshita, S. Kanemura, D. Itoh, T. Sugiki, M. Okumura, A. Ramamoorthy, Y.-H. Lee, Impact of membrane curvature on amyloid aggregation, Biochim. Biophys. Acta BBA - Biomembr., 1860 (2018) 1741–1764.

[10] S.M. Butterfield, H.A. Lashuel, Amyloidogenic Protein–Membrane Interactions: Mechanistic Insight from Model Systems, Angew. Chem. Int. Ed., 49 (2010) 5628–5654.

[11] J.D. Harper, S.S. Wong, C.M. Lieber, P.T. Lansbury, Observation of metastable Aβ amyloid protofibrils by atomic force microscopy, Chem. Biol., 4 (1997) 119–125.

[12] C. Ionescu-Zanetti, R. Khurana, J.R. Gillespie, J.S. Petrick, L.C. Trabachino, L.J. Minert, S.A. Carter, A.L. Fink, Monitoring the assembly of Ig light-chain amyloid fibrils by atomic force microscopy, Proc. Natl. Acad. Sci., 96 (1999) 13175–13179.

[13] M. Wahlbom, X. Wang, V. Lindström, E. Carlemalm, M. Jaskolski, A. Grubb, Fibrillogenic Oligomers of Human Cystatin C Are Formed by Propagated Domain Swapping*, J. Biol. Chem., 282 (2007) 18318–18326.

[14] P. Jurczak, E. Sikorska, P. Czaplewska, S. Rodziewicz-Motowidlo, I. Zhukov, A. Szymanska, The Influence of the Mixed DPC:SDS Micelle on the Structure and Oligomerization Process of the Human Cystatin C, Membranes, 11 (2021) 17.

[15] P. Jurczak, K. Szutkowski, S. Lach, S. Jurga, P. Czaplewska, A. Szymanska, I. Zhukov, DMPC Phospholipid Bilayer as a Potential Interface for Human Cystatin C Oligomerization: Analysis of Protein-Liposome Interactions Using NMR Spectroscopy, Membranes, 11 (2021) 13.

[16] M. Beseničar, P. Maček, J.H. Lakey, G. Anderluh, Surface plasmon resonance in protein–membrane interactions, Chem. Phys. Lipids, 141 (2006) 169–178.

[17] M.J. Swamy, R.S. Sankhala, B.P. Singh, Thermodynamic Analysis of Protein–Lipid Interactions by Isothermal Titration Calorimetry, in: J.H. Kleinschmidt (Ed.), Lipid-Protein Interact. Methods Protoc., Springer, New York, NY, 2019: pp. 71–89.

[18] S.A. Tatulian, FTIR Analysis of Proteins and Protein–Membrane Interactions, in: J.H. Kleinschmidt (Ed.), Lipid-Protein Interact. Methods Protoc., Springer, New York, NY, 2019: pp. 281–325.

[19] O. Vadas, M.L. Jenkins, G.L. Dornan, J.E. Burke, Chapter Seven - Using Hydrogen–Deuterium Exchange Mass Spectrometry to Examine Protein–Membrane Interactions, in: M.H. Gelb (Ed.), Methods Enzymol., Academic Press, 2017: pp. 143–172.
[20] E.E. Scott, C.R. Wolf, M. Otyepka, S.C. Humphreys, J.R. Reed, C.J. Henderson, L.A. McLaughlin, M. Paloncyova, V. Navratilova, K. Berka, P. Anzenbacher, U.P. Dahal, C. Barnaba, J.A. Brozik, J.P. Jones, F. Estrada, J.S. Laurence, J.W. Park, W.L. Backes, The Role of Protein-Protein and Protein-Membrane Interactions on P450 Function, Drug Metab. Dispos., (2016).
[21] S.B. Nielsen, D.E. Otzen, Quartz Crystal Microbalances as Tools for Probing Protein–Membrane Interactions, in: J.H. Kleinschmidt (Ed.), Lipid-Protein Interact. Methods Protoc., Springer, New York, NY, 2019: pp. 31–52.
[22] C. Aisenbrey, M. Michalek, E.S. Salnikov, B. Bechinger, Solid-State NMR Approaches to Study Protein Structure and Protein–Lipid Interactions, in: J.H. Kleinschmidt (Ed.), Lipid-Protein Interact. Methods Protoc., Humana Press, Totowa, NJ, 2013: pp. 357–387.
[23] R.A.S. Smith, A. Nabok, B.J.F. Blakeman, W.-F. Xue, B. Abell, D.P. Smith, Analysis of Toxic Amyloid Fibril Interactions at Natively Derived Membranes by Ellipsometry, PLOS ONE, 10 (2015) e0132309.
[24] D.J. Lindberg, E. Wesén, J. Björkeroth, S. Rocha, E.K. Esbjörner, Lipid membranes catalyse the fibril formation of the amyloid-β (1–42) peptide through lipid-fibril interactions that reinforce secondary pathways, Biochim. Biophys. Acta BBA - Biomembr., 1859 (2017) 1921–1929.
[25] K. Sasahara, K. Morigaki, K. Shinya, Amyloid aggregation and deposition of human islet amyloid polypeptide at membrane interfaces, FEBS J., 281 (2014) 2597–2612.
[26] L.L. Martin, C. Kubeil, S. Piantavigna, T. Tikkoo, N.P. Gray, T. John, A.N. Calabrese, Y. Liu, Y. Hong, M.A. Hossain, N. Patil, B. Abel, R. Hoffmann, J.H. Bowie, J.A. Carver, Amyloid aggregation and membrane activity of the antimicrobial peptide uperin 35, Pept. Sci., 110 (2018) e24052.
[27] X. Dong, Q. Qiao, Z. Qian, G. Wei, Recent computational studies of membrane interaction and disruption of human islet amyloid polypeptide: Monomers, oligomers and protofibrils, Biochim. Biophys. Acta BBA - Biomembr., 1860 (2018) 1826–1839.
[28] Z. Lv, M. Hashemi, S. Banerjee, K. Zagorski, J.-C. Rochet, Y.L. Lyubchenko, Assembly of α-synuclein aggregates on phospholipid bilayers, Biochim. Biophys. Acta BBA - Proteins Proteomics, 1867 (2019) 802–812.
[29] A. Quist, I. Doudevski, H. Lin, R. Azimova, D. Ng, B. Frangione, B. Kagan, J. Ghiso, R. Lal, Amyloid ion channels: A common structural link for protein-misfolding disease, Proc. Natl. Acad. Sci., 102 (2005) 10427–10432.
[30] D. Desai, A. Kumar, D. Bose, M. Datta, Ultrasensitive sensor for detection of early stage chronic kidney disease in human, Biosens. Bioelectron., 105 (2018) 90–94.
[31] K.S.S. Devi, U.M. Krishnan, Microfluidic electrochemical immunosensor for the determination of cystatin C in human serum, Microchim. Acta, 187 (2020) 585.
[32] E.K.G. Trindade, B.V.M. Silva, R.F. Dutra, A probeless and label-free electrochemical immunosensor for cystatin C detection based on ferrocene functionalized-graphene platform, Biosens. Bioelectron., 138 (2019) 111311.
[33] R.S. Gomes, B.A. Gomez-Rodríguez, R. Fernandes, M.G.F. Sales, F.T.C. Moreira, R.F. Dutra, Plastic Antibody of Polypyrrole/Multiwall Carbon Nanotubes on Screen-Printed Electrodes for Cystatin C Detection, Biosensors, 11 (2021) 175.
[34] P.A.B. Ferreira, M.C.M. Araujo, C.M. Prado, R.A. de Lima, B.A.G. Rodríguez, R.F. Dutra, An ultrasensitive Cystatin C renal failure immunosensor based on a PPy/CNT electrochemical capacitor grafted on interdigitated electrode, Colloids Surf. B Biointerfaces, 189 (2020) 110834.
[35] L.J.C. Jeuken, S.D. Connell, M. Nurnabi, J. O'Reilly, P.J.F. Henderson, S.D. Evans, R.J. Bushby, Direct Electrochemical Interaction between a Modified Gold Electrode and a Bacterial Membrane Extract, Langmuir, 21 (2005) 1481–1488.

[36] D. Mrdenovic, Z. Su, W. Kutner, J. Lipkowski, P. Pieta, Alzheimer's disease-related amyloid β peptide causes structural disordering of lipids and changes the electric properties of a floating bilayer lipid membrane, Nanoscale Adv., 2 (2020) 3467–3480.
[37] M. Abrahamson, H. Dalbøge, I. Olafsson, S. Carlsen, A. Grubb, Efficient production of native, biologically active human cystatin C by Escherichia coli, FEBS Lett., 236 (1988) 14–18.
[38] J. Kloubek, Development of methods for surface free energy determination using contact angles of liquids on solids, Adv. Colloid Interface Sci., 38 (1992) 99–142.
[39] D.K. Owens, R.C. Wendt, Estimation of the surface free energy of polymers, J. Appl. Polym. Sci., 13 (1969) 1741–1747.
[40] A. Cirocka, D. Zarzeczańska, A. Wcisło, J. Ryl, R. Bogdanowicz, B. Finke, T. Ossowski, Tuning of the electrochemical properties of transparent fluorine-doped tin oxide electrodes by microwave pulsed-plasma polymerized allylamine, Electrochimica Acta, 313 (2019) 432–440.
[41] M. Maszota-Zieleniak, P. Jurczak, M. Orlikowska, I. Zhukov, D. Borek, Z. Otwinowski, P. Skowron, Z. Pietralik, M. Kozak, A. Szymańska, S. Rodziewicz-Motowidło, NMR and crystallographic structural studies of the extremely stable monomeric variant of human cystatin C with single amino acid substitution, FEBS J., 287 (2020) 361–376.
[42] X. Xu, A. Makaraviciute, S. Kumar, C. Wen, M. Sjödin, E. Abdurakhmanov, U.H. Danielson, L. Nyholm, Z. Zhang, Structural Changes of Mercaptohexanol Self-Assembled Monolayers on Gold and Their Influence on Impedimetric Aptamer Sensors, Anal. Chem., 91 (2019) 14697–14704.
[43] T. Swebocki, P. Niedziałkowski, A. Cirocka, E. Szczepańska, T. Ossowski, A. Wcisło, In pursuit of key features for constructing electrochemical biosensors – electrochemical and acid-base characteristic of self-assembled monolayers on gold, Supramol. Chem., 32 (2020) 256–266.
[44] G. Chen, W. Chen, L. Xu, H. Jin, W. Sun, J. Lan, F. Wu, X. Zhang, J. Zhang, J. Chen, Sensitive, Highly Stable, and Anti-Fouling Electrode with Hexanethiol and Poly-A Modification for Exosomal microRNA Detection, Anal. Chem., 94 (2022) 5382–5391.
[45] P. Niedziałkowski, M. Bojko, J. Ryl, A. Wcisło, M. Spodzieja, K. Magiera-Mularz, K. Guzik, G. Dubin, T.A. Holak, T. Ossowski, S. Rodziewicz-Motowidło, Ultrasensitive electrochemical determination of the cancer biomarker protein sPD-L1 based on a BMS-8-modified gold electrode, Bioelectrochemistry, 139 (2021) 107742.
[46] M. Keough, J.F. McLeod, T. Salomons, P. Hillen, Y. Pei, G. Gibson, K. McEleney, R. Oleschuk, Z. She, Realizing new designs of multiplexed electrode chips by 3-D printed masks, RSC Adv., 11 (2021) 21600–21606.
[47] R. Levicky, T.M. Herne, M.J. Tarlov, S.K. Satija, Using Self-Assembly To Control the Structure of DNA Monolayers on Gold: A Neutron Reflectivity Study, J. Am. Chem. Soc., 120 (1998) 9787–9792.
[48] X. Xu, Y. Yu, Q. Hu, S. Chen, L. Nyholm, Z. Zhang, Redox Buffering Effects in Potentiometric Detection of DNA Using Thiol-Modified Gold Electrodes, ACS Sens., 6 (2021) 2546–2552.
[49] S.A. Lincy, V. Dharuman, P. Kumar, Ultrasensitive and direct detection of DNA and whole E coli cell at cholesterol gold nanoparticle composite film electrode, Ionics, 28 (2022) 1973–1984.
[50] R.K. Shervedani, A. Farahbakhsh, M. Bagherzadeh, Functionalization of gold cysteamine self-assembled monolayer with ethylenediaminetetraacetic acid as a novel nanosensor, Anal. Chim. Acta, 587 (2007) 254–262.
[51] G.D. McEwen, F. Chen, A. Zhou, Immobilization, hybridization, and oxidation of synthetic DNA on gold surface: Electron transfer investigated by electrochemistry and scanning tunneling microscopy, Anal. Chim. Acta, 643 (2009) 26–37.
[52] R.P. Janek, W.R. Fawcett, A. Ulman, Impedance Spectroscopy of Self-Assembled Monolayers on Au(111): Sodium Ferrocyanide Charge Transfer at Modified Electrodes, Langmuir, 14 (1998) 3011–3018.